Supporting information

Sulfur dioxide exploitation by electrochemical oxidation of sulfite in near-neutral pH electrolytes: A kinetics and mechanistic approach

R.A. Márquez-Montes[a], R.E. Orozco-Mena[a], D. Lardizábal-Gutiérrez[b], D. Chávez-Flores[a], A. López-Ortíz[b], and V.H. Ramos-Sánchez[*a]

[a]*Cuerpo Académico de Química Aplicada y Educativa, Facultad de Ciencias Químicas, Universidad Autónoma de Chihuahua, Nuevo Campus Universitario, Circuito Universitario, Chihuahua, Chih., C.P. 31125, México.*

[b]*Centro de Investigación en Materiales Avanzados, S.C., Miguel de Cervantes #120, Complejo Industrial Chihuahua, Chih., C.P. 31136, México.*

*Corresponding author, e-mail: vramos@uach.mx

1. Analysis of bare GCE

An analysis of the bare glassy carbon is performed to compare measurements of Pd-coated electrodes. Fig. S1 shows the electrooxidation of 50 mM sulfite solutions on bare glassy carbon at 400 rpm. A well-defined current response is observed without reduction peaks in the cathodic return sweep. Oxidation starts around 0.18 V in both electrolytes, nearly 0.1 V beyond the onset potential observed with Pd-coated electrodes. Thus, it is evident that Pd decreases the onset potential of sulfite oxidation in contrast to glassy carbon. Both electrolytes show an oxidation peak around 0.8 V, where sodium sulfite exhibits a higher associated current. This behavior correlates observed differences in limiting current values between Fig. 2a and Fig. 2b in the main document. Note: to compare current intensities with Fig. 2, a loading mass of 4 µg Pd must be considered since curves of Fig. 2a and Fig. 2b are expressed in terms of electrocatalyst mass.

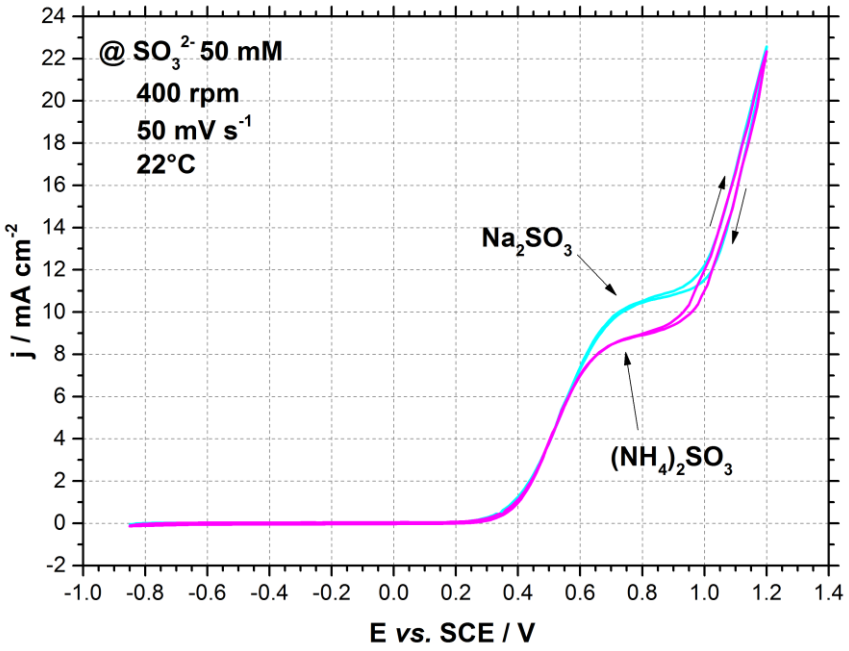

Fig. S1. Potential-current curves of the electrooxidation of 50 mM sulfite on a rotating, glassy carbon electrode.

2. Temperature dependence analysis

2.1. Anodic charge transfer coefficients and reaction order

Dependence of β with temperature in the first Tafel slope region (0.10 to 0.28 V) is shown in Fig. S2. Variation of β at low potentials is similar for both electrolytes. Near 50°C, β stabilizes around 0.23.

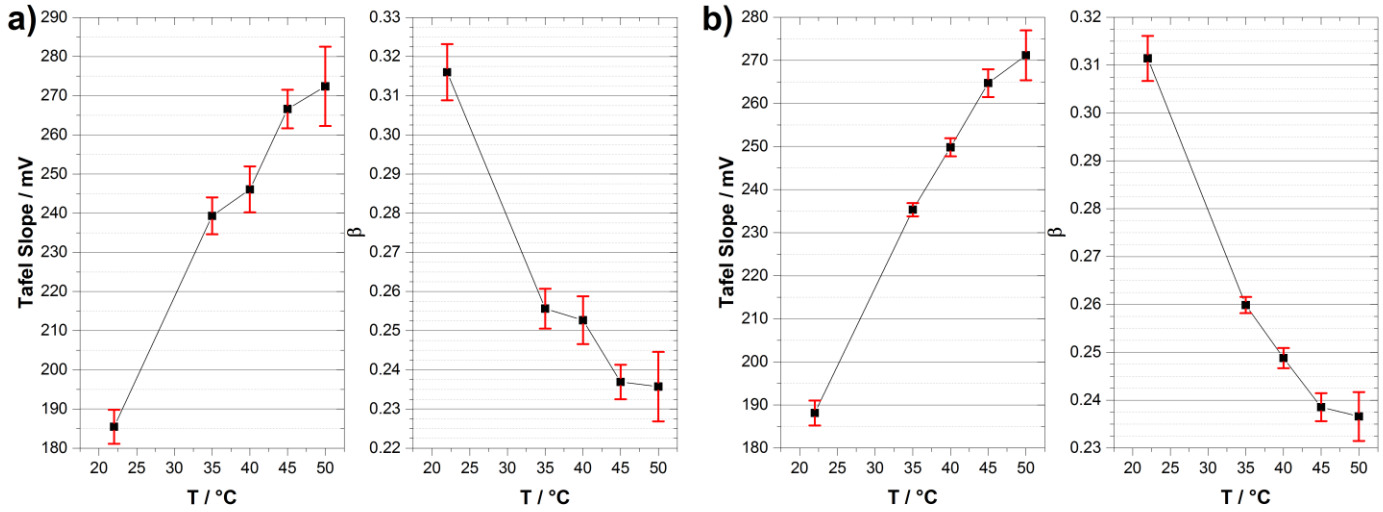

Fig. S2. Temperature dependence of Tafel slopes and β in the low potential region for a) ammonium and b) sodium electrolytes. Error bars show the variation due to rotation rates.

Dependence of β with temperature in the second Tafel slope region (0.40 to 0.80 V) is shown in Fig. S3. β remains almost constant around 0.19, especially in sodium sulfite. Ammonium sulfite exhibits an atypical decrease down to β = 0.16, which is fairly low.

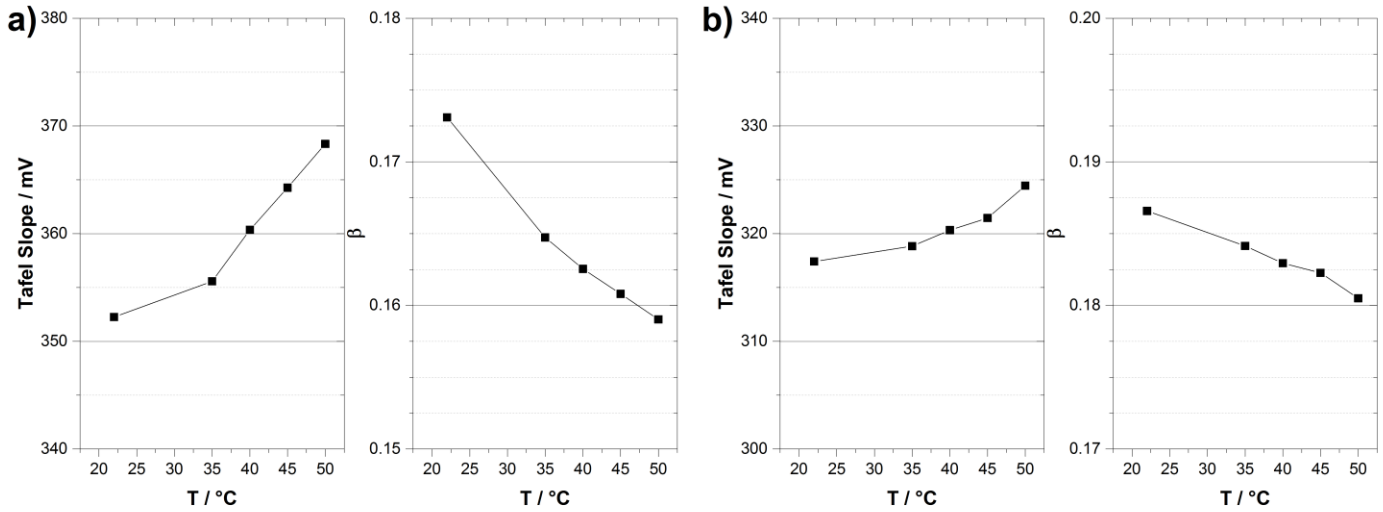

Fig. S3. Temperature dependence of Tafel slopes and β in the high potential region for a) ammonium and b) sodium electrolytes.

Dependence of reaction orders with potential and temperature is shown in Fig. S4. Fractional reaction orders increase from below 1 to almost 2. Note that reaction order suddenly increases between 0.50 and 0.60 V, and it stabilizes *ca.* 0.60 V in ammonium sulfite. In sodium sulfite, reaction order increases progressively until it stabilizes around 0.75 V. Additionally, reaction order is independent of temperature, since error bars exhibit comparable behaviors despite temperature changes.

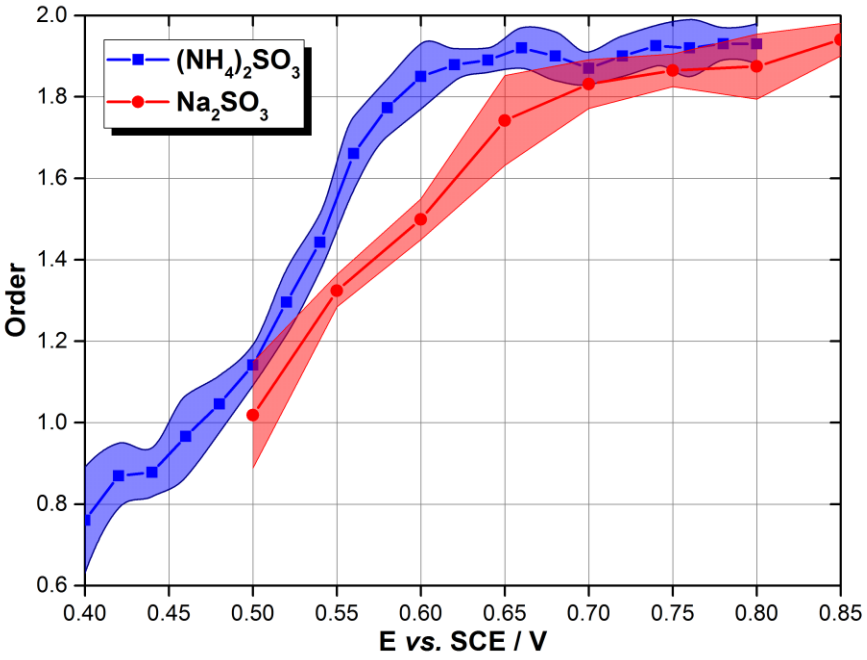

Fig. S4. Plot of reaction orders against potential for both electrolytes. Error bars show the variation due to temperature.

2.2. Activation energy studies

The approach proposed by Protsenko & Danilov [1] is used to obtain activation energies, since sulfite electrooxidation is a irreversible electrochemical reaction controlled by both kinetics and diffusion. A brief understanding of the mathematical formulation is given, and linearization models are proposed to obtain activation energies from experimental data.

The general definition of the formal activation energy is shown in Eq. (S1):

$$\left(\frac{\partial \ln j}{\partial \ln T}\right)_{E,c_i} = \frac{\Omega}{RT^2} \tag{S1}$$

where j is the current density, T is the absolute temperature, R is the universal gas constant, c_i is the molar concentration of species *i*, E is the electrode potential, and Ω is the formal activation energy. A simple redox reaction can be established as follows:

$$\mathrm{Ox} + \mathrm{ne}^- \leftrightarrow \mathrm{Red} \tag{S2}$$

Hence, Eq. (S1) can be defined for direct (cathodic) and reverse (anodic) reactions:

$$\left(\frac{\partial \ln \vec{j}}{\partial \ln T}\right)_{E,c_i} = \frac{\vec{\Omega}}{RT^2}; \quad \left(\frac{\partial \ln \overleftarrow{j}}{\partial \ln T}\right)_{E,c_i} = \frac{\overleftarrow{\Omega}}{RT^2} \tag{S3}$$

After certain assumptions and mathematical simplification [1], Ω is defined in terms of the charge transfer coefficient, as shown in Eq. (S4) and Eq. (S5) for cathodic and anodic reactions, respectively:

$$\vec{\Omega} = \vec{\Omega}_0 + \alpha nFE \tag{S4}$$

$$\overleftarrow{\Omega} = \overleftarrow{\Omega}_0 + \beta nFE \tag{S5}$$

where Ω_0 is the formal activation energy at $E = 0$, n is the number of electrons transferred, α is the cathodic charge transfer coefficient, β is the anodic charge transfer coefficient, and F is the Faraday's constant. Let us consider only the reverse reaction (anodic current will be considered as positive). If the electrode process occurs at an anodic potential far from the equilibrium, the current density expression in an excess of supporting electrolyte and steady-state diffusion can be written as follows:

$$j = \frac{nFk_s^0 c_{Red} \exp\left[-\frac{\beta nF(E-E^0)}{RT}\right]}{1 + \frac{k_s^0 \exp\left[-\frac{\beta nF(E-E^0)}{RT}\right]}{k_D}} \tag{S6}$$

where k_s^0 is the heterogeneous rate constant, c_{Red} is the bulk concentration of Red, E^0 is the standard electrode potential, and k_D is the mass transfer coefficient. Note that the kinetic component is defined by k_s^0, whereas the mass transfer by k_D. Both terms depend on temperature (as well as E^0).

Temperature dependence of k_s^0 is shown in Eq. (S7)

$$k_s^0 = k^0 \exp\left[-\frac{\beta n F E^0}{RT}\right] = J_0 \exp\left[-\frac{\Omega_0}{RT}\right] \exp\left[-\frac{\beta n F E^0}{RT}\right] \quad \text{(S7)}$$

where k^0 is the rate constant for the charge transfer at $E = 0$, and J_0 is the charge transfer pre-exponential factor. Temperature dependence of k_D, is shown in Eq. (S8):

$$k_D = J_D \exp\left[-\frac{Z_D}{RT}\right] \quad \text{(S8)}$$

where Z_D is the diffusion mass transfer activation energy and J_D is the mass transfer pre-exponential factor. Note that variables such as k_s^0, k^0, J_0, J_D, and Z_D must be specified for cathodic or anodic reactions. For sake of simplicity, here we only consider the anodic reaction, so these variables define anodic processes related to Red as a reagent.

Valid current density relationships must be satisfied. k_s^0 is associated to the current of discharge stage, *i.e.* the kinetics-controlled current density, j_k:

$$j_k = nFk_s c_{Red} = nFk_s^0 c_{Red} \exp\left[-\frac{\beta n F (E - E^0)}{RT}\right]; \quad k_s = k_s^0 \exp\left[-\frac{\beta n F (E - E^0)}{RT}\right] \quad \text{(S9)}$$

where k_s is a general heterogeneous rate constant (which includes temperature-dependent terms). By substituting Eq. (S7) into Eq. (S9), the dependence of j_k with Ω is obtained:

$$j_k = nFJ_0 c_{Red} \exp\left[-\frac{\beta n F (E - E^0)}{RT}\right] \exp\left[-\frac{\Omega_0}{RT}\right] \exp\left[-\frac{\beta n F E^0}{RT}\right] = nFJ_0 c_{Red} \exp\left[-\frac{\Omega}{RT}\right] \quad \text{(S10)}$$

The diffusion mass transfer rate constant is associated to the limiting current density, j_L:

$$j_L = nFk_D c_{Red} \quad \text{(S11)}$$

By substituting Eq. (S8) into Eq. (S11), the dependence of j_L with Z_D is obtained:

$$j_L = nFc_{Red} J_D \exp\left[-\frac{Z_D}{RT}\right] \quad \text{(S12)}$$

Hence, electrochemical processes depend on two energy barriers, which altogether compose the apparent activation energy Ω_{App} as follows:

$$\Omega_{App} = RT^2 \left(\frac{\partial \ln j}{\partial T}\right)_{E,c_i} = \frac{k_D(\Omega_0 + \beta n F E) + Z_D k_s^0 \exp\left[-\frac{\beta n F (E - E^0)}{RT}\right]}{k_D + k_s^0 \exp\left[-\frac{\beta n F (E - E^0)}{RT}\right]} = \frac{j_L \Omega + j_k Z_D}{j_L + j_k} \quad \text{(S13)}$$

Ω_{App} is the weighted arithmetic mean between Ω and Z_D. Hence, these parameters can be obtained by kinetic and mass transfer-limited scenarios. If the reaction is mass transfer-limited:

$$k_s^0 \exp\left[-\frac{\beta n F (E - E^0)}{RT}\right] \gg k_D \quad \text{(S14)}$$

Increase of the temperature only improves k_D (*i.e.*, $\Omega_{App} = Z_D$). If the reaction is kinetics-controlled:

$$k_s^0 \exp\left[-\frac{\beta nF(E-E^0)}{RT}\right] \ll k_D \quad \text{(S15)}$$

Increase of the temperature only improves the charge transfer (*i.e.*, $\Omega_{App} = \Omega_0 + \beta nFE = \Omega$). Hence, Ω_{App} decreases linearly when shifting the electrode potential in the anodic direction. Note that a plot of Ω against E gives β as the slope, and such graph also allows to define if β varies with potential.

Experimental determination of Z_D and Ω is achieved when j_L and j_k are known (the latter at different E). Eq. (S10) and Eq. (S12) are linearized as follows:

$$\ln(j_k) = -\frac{\Omega}{RT} + \ln(nFc_{Red}J_0) \quad \text{(S16)}$$

$$\ln(j_L) = -\frac{Z_D}{RT} + \ln(n\mathrm{Fc_{Red}}J_D) \quad \text{(S17)}$$

If k_D is known, and since $k_D = D/\delta$ (where D is the diffusion coefficient and δ is the thickness of the diffusion layer), Eq. (S8) can be linearized as follows:

$$\ln(D) = -\frac{Z_D}{RT} + \ln(J_D\delta) \quad \text{(S18)}$$

Activation energies are obtained from potential-current data using Eqs. (S16)-(S18), whereas Ω_{App} is calculated using Eq. (S13). Fig. S5 shows plots of Ω_{App} against E from our experimental results. Note that Ω_{App} decreases progressively until a horizontal asymptote at sufficiently anodic potentials begins. This is because condition of Eq. (S14) is achieved. Since linear segments correspond to Tafel regions, a change in the slope around 0.35 V is attributed to a reaction mechanism change.

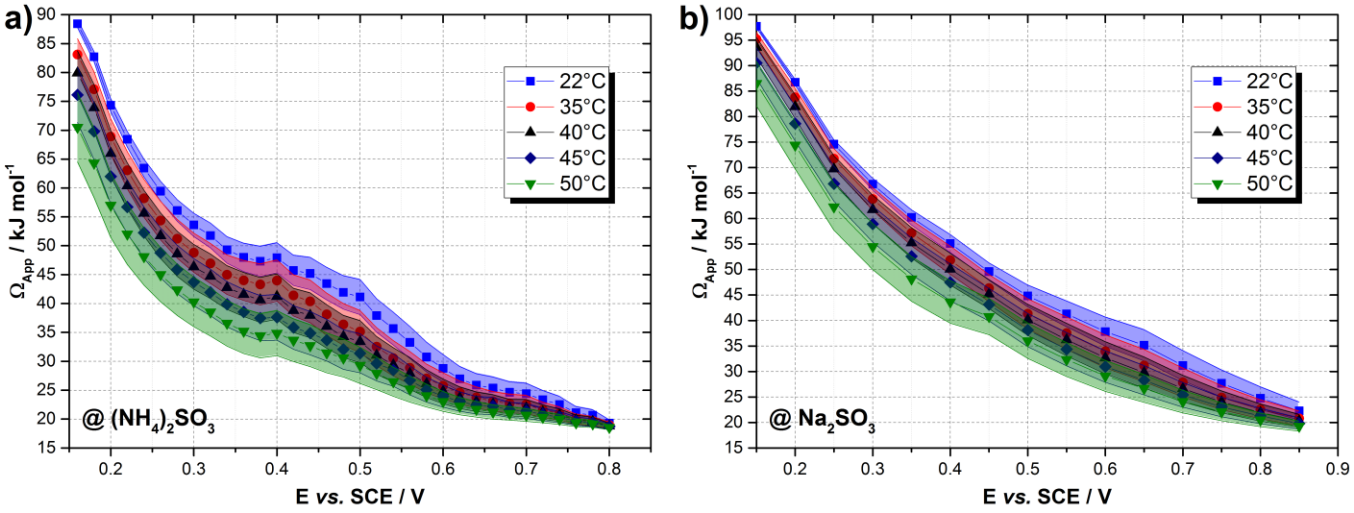

Fig. S5. Ω_{App} as a function of E for a) ammonium and b) sodium electrolytes.

3. Sulfite electrooxidation mechanism

3.1 *Composition of aqueous solutions of S(IV) species and its dependence on pH*

A detailed discussion about S(IV) speciation is described elsewhere [2-4]. Specifically, the following insights can be made from S(IV) speciation at near-neutral pH:

- Sulfite solutions are composed by mixtures of sulfite/bisulfite ions: below pH 6, bisulfite is predominant; whereas above pH 8, sulfite is expected to be the major component.
- If ammonium salts are used, a lower pH is reached. Moreover, aqueous ammonia becomes an important component of the mixture above pH 9 (thus, ammonia can evolve from solution).

Since pH values are the only significant difference between ammonium and sodium electrolytes, the role of such parameter is addressed.

3.2 *Overview of sulfite electrooxidation pathways*

Bisulfite ions can be oxidized into sulfate according to the following overall reaction [5, 6]:

$$\mathrm{HSO_3^-} + \mathrm{H_2O} \rightleftarrows \mathrm{SO_4^{2-}} + 3\mathrm{H^+} + 2\mathrm{e^-};\ \ \mathrm{E_0} = 0.105\ \mathrm{V}\ vs.\ \mathrm{SHE} \qquad (\mathrm{S19})$$

In acid solutions, where aqueous sulfur dioxide and bisulfite ions are present, proposed mechanisms consist of a two-step charge transfer [7]. First, one electron is transferred through the formation of a bisulfite radical by adsorbed bisulfite, then the second electron is transferred:

$$\mathrm{HSO_{3(ad)}^-} \rightarrow \mathrm{HSO_3^*} + \mathrm{e^-} \qquad (\mathrm{S20})$$

$$\mathrm{HSO_3^*} + \mathrm{H_2O} \rightarrow \mathrm{SO_4^{2-}} + 3\mathrm{H^+} + \mathrm{e^-} \qquad (\mathrm{S21})$$

In sodium sulfite electrooxidation experiments on graphite [7], a maximum peak of current near 1.00 V *vs.* SHE (0.76 V *vs.* SCE) was related to bisulfite electrooxidation. Furthermore, it was suggested that in acid media bisulfite electrooxidation occurs in bulk, whereas in alkaline media it proceeds near the electrode surface. Indeed, even the slightest acidification of alkaline media, modifies the voltammetric response. This behavior was confirmed at a wide pH range, clearly differentiating a

sulfite electrooxidation peak at 0.60 V *vs.* SHE (0.36 V *vs.* SCE) above pH 12, and a bisulfite peak below pH 5. At near-neutral pH, both species exhibited electrooxidation peaks.

Regarding the kinetic nature of both ions, it has been extensively accepted that electrooxidation of sulfite and bisulfite usually proceeds through fast and weak adsorption processes [5, 7-10]. Especially, sulfite electrooxidation mechanisms at alkaline conditions are validated as catalytic adsorption reaction pathways by available kinetic data for graphite [8], and platinum [9, 11]. However, there is a lack of kinetic studies regarding bisulfite electrooxidation at mild acidic conditions.

Regarding the mass transfer, both ions proceed at the same diffusion rate [7], and even though diffusion coefficients available in the literature are in the same order of magnitude, complex pH profiles between the bulk and the diffusion layer hinders the diffusion effect, especially when a remarkable pH gradient is evident [5]. In the present work, a buffer inhibits such pH gradient.

On the other hand, sulfite reaction mechanism is not avidly investigated. Skavås and Hemmingsen [9] concluded that the sulfite electrooxidation rate at pH 11 involves the oxidation of adsorbed sulfite into a sulfite radical:

$$SO_{3\,(ad)}^{2-} \rightarrow SO_{3\,(ad)}^{*-} + e^{-} \tag{S22}$$

Fractional orders indicate that the abovementioned step is the rate-determining step (rds). The following step involves the reaction of two sulfite radicals to yield dithionate, which in turn is decomposed into sulfite and sulfate:

$$2SO_{3\,(ad)}^{*-} \rightarrow S_2O_{6\,(ad)}^{2-} \tag{S23}$$

$$S_2O_{6\,(ad)}^{2-} + 2OH^{-} \rightarrow SO_{3\,(ad)}^{2-} + SO_{4\,(ad)}^{2-} + H_2O \tag{S24}$$

At high potentials, the mechanism consist of desorption of sulfite radicals into solution, resulting in a mechanism analogue to Eq. (S23) and Eq. (S24). The potential threshold defined by β change is 0.62 V vs. SCE, which implies that below such potential adsorption occurs, whereas at higher potentials desorption takes place [9]. The latter was also confirmed in a wall-jet flow cell [11].

A similar mechanism is proposed on graphite at pH 12 by Lu *et al*. [8], in which adsorbed sulfite is oxidized into sulfite radical at low potentials. This is supported due to a constant Tafel slope of 60 mV and a non-linear reaction order below 1. Eq. (S23) was considered the rds, followed by desorption of sulfite radicals and further oxidation in presence of hydroxide:

$$SO_3^{*-} + 2OH^- \rightarrow SO_4^{2-} + H_2O + e^- \quad (S25)$$

In this study, sulfite adsorption was considered negligible above 0.40 V *vs.* SCE (*i.e.,* sulfite is directly oxidized on the surface through a mechanism where the first step is analogue to Eq. (S23) and the second step is Eq. (S25)). This conclusion is supported by a Tafel slope of 200 mV and first-order behavior. As a result, previous studies agree that certain reaction pathways might not entirely consist in adsorption steps, especially at high potentials where direct oxidation occurs [8, 9, 11].

Dithionate is considered as intermediate of sulfur species by similar studies [9, 12, 13]. It acts as inhibitor of S(IV) species electrooxidation by depleting oxide-free sites on gold, resulting in competitive adsorption of side-reaction oxidation products [10]. Other spectroscopic [14] and voltammetric studies [15] report simultaneous formation of dithionate and sulfate on Pt and PtO. Additionally to Eq. (S24), formation of dithionate also occurs by charge transfer reactions [10, 12, 16]:

$$2HSO_3^- \rightarrow S_2O_6^{2-} + 2H^+ + 2e^- \quad (S26)$$

$$2SO_3^{2-} \rightarrow S_2O_6^{2-} + 2e^- \quad (S27)$$

Dithionate yield is not dependent on sulfite concentration nor temperature, but on electrode composition and pH. Maximum yields are reported around pH 7, being gold the most susceptible material with yields up to 30% [17]. This behavior is due to different mechanisms influenced by pH.

Based on the available sulfite electrooxidation pathways reported in the literature, an integrated overview of reaction mechanisms at near-neutral pH is shown in Fig. S6. Routes prone to occur at acidic and alkaline conditions are shown, as well as adsorption and bulk reactions.

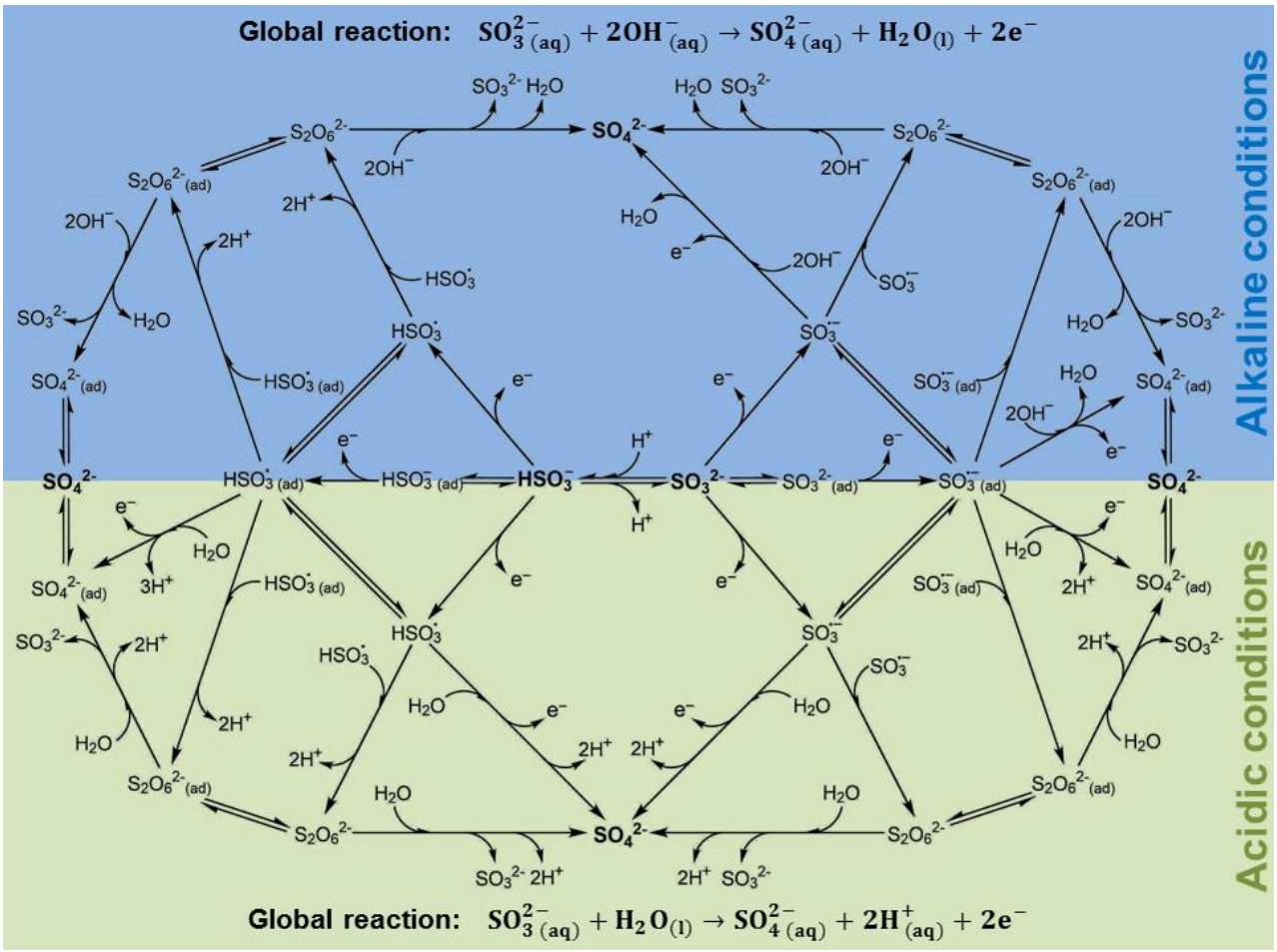

Fig. S6. Overview of sulfite electrooxidation mechanisms in mildly acidic and alkaline media.

For our validation, chemical reactions at extreme acidic conditions are not considered. Thus, SO_2 oxidation, bisulfate occurrence and homolytic cleavage of dithionate are all neglected [18, 19]. All routes within the diagram lead to sulfate as the overall product. Dissociation and adsorption equilibria are considered since some reaction pathways might proceed by these means based on particular conditions, as already described. It is noteworthy to mention that overall electrooxidation reactions always lead to Eq. (1) or Eq. (2) in the main document, despite the selected route.

3.3 *Multi-step theory approximation for mechanism validation*

Considering the theory of multistep electrode reactions and the steady-state approximation [20-22], pathways in Fig. S6 are tested in order to correlate kinetic evidence found in this study. Such approximations are based on the following rationale:

- Protons or hydroxide ions are not involved in the rds due to pH control, as stated by previous studies [8, 9]. Thereby, rate expressions only involve sulfur species.
- The rds is controlled by an electrochemical step.
- Reverse reactions of pure adsorption steps are neglected since the rds is not at equilibrium.

The calculation method is shown as follows using the mechanism validated in the main article:

Step 1: $SO_{3\,(aq)}^{2-} \rightleftarrows SO_{3\,(ad)}^{2-}$

Step 2: $SO_{3\,(ad)}^{2-} \rightarrow SO_{3\,(ad)}^{*-} + e^{-}$

Step 3: $2SO_{3\,(ad)}^{*-} \rightarrow S_2O_{6\,(ad)}^{2-}$

Step 4: $S_2O_{6\,(ad)}^{2-} + 2OH^{-} \rightarrow SO_{3\,(ad)}^{2-} + SO_{4\,(ad)}^{2-} + H_2O$

Rate expressions for each step are defined according to the molecularity of the reaction (where θ_s represents the free surface fraction, and $f = F/RT$):

$$r_1 = k_1 c_{SO_{3\,(aq)}^{2-}} \theta_s \; ; \qquad r_{-1} = k_{-1} \theta_{SO_{3\,(ad)}^{2-}} \tag{S28}$$

$$r_2 = k_2 \theta_{SO_{3\,(ad)}^{2-}} \exp(\beta f E) \; ; \qquad r_{-2} = k_{-2} \theta_{SO_{3\,(ad)}^{*-}} \exp[-\alpha f E] \tag{S29}$$

$$r_3 = k_3 \theta_{SO_{3\,(ad)}^{*-}}^2 \; ; \qquad r_{-3} = k_{-3} \theta_{S_2O_{6\,(ad)}^{2-}} \tag{S30}$$

$$r_4 = k_4 \theta_{S_2O_{6\,(ad)}^{2-}} c_{OH^-}^2 \; ; \qquad r_{-4} = k_{-4} \theta_{SO_{3\,(ad)}^{2-}} \theta_{SO_{4\,(ad)}^{2-}} \tag{S31}$$

The following observations are made:

- Only Step 2 is electrochemical.
- Rate expression of Eq. (S31), depends on hydroxide ions. Our experimental results suggest that the rds does not involve hydroxide ions.
- Reverse reaction of Step 4 is not likely to occur because sulfate tends to desorb.
- Step 3 is second-order respect to sulfite radical.

If Step 2 is chosen as the rds, then $k_{-2} = 0$ and the reverse reaction (r_{-2}) is neglected. Overall mass balances for involved species are established (where $R_i = dc_i/dt$):

$$R_{SO_{3\,(aq)}^{2-}} = r_4 + r_{-1} - r_1 \tag{S32}$$

$$R_{SO_{3\,(ad)}^{2-}} = \; r_1 - r_{-1} - r_2 \tag{S33}$$

$$R_{SO_{3\,(ad)}^{*-}} = \; r_2 + 2r_{-3} - r_3 \tag{S34}$$

$$R_{S_2O_{6\,(ad)}^{2-}} = r_3 - 2r_{-3} - r_4 \quad (S35)$$

$$R_{SO_{4\,(ad)}^{2-}} = r_4 \quad (S36)$$

The objective is to demonstrate that the rate expression of sulfate production is defined by an expression of the rds, since it controls the overall reaction rate. In order to solve the final rate expression, simultaneous solving of the equation system is required.

Steady-state approximations (SSA) are used if the equation system is complex. SSA establishes that after a very short interval of time, any reactive intermediate will reach a steady concentration, *i.e.* its formation rate equals the consumption rate. Since only the reagent of the rds does not fulfill this approximation, any other intermediate mass balance is almost 0. For instance, Eq. (S35) becomes:

$$R_{S_2O_{6\,(ad)}^{2-}} = r_3 - 2r_{-3} - r_4 = 0 \quad (S37)$$

If Eqs. (S30)-(S31) are substituted into Eq. (S37), $\theta_{S_2O_{6\,(ad)}^{2-}}$ is obtained:

$$\theta_{S_2O_{6\,(ad)}^{2-}} = \frac{k_3 \theta_{SO_{3\,(ad)}^{*-}}^2}{k_4 c_{OH^-}^2 + 2k_{-3}} \quad (S38)$$

The sulfite radical can be considered as a reactive intermediate, thus:

$$R_{SO_{3\,(ad)}^{*-}} = r_2 + 2r_{-3} - r_3 = 0 \quad (S39)$$

$$\theta_{SO_{3\,(ad)}^{*-}} = \frac{\sqrt{k_2 k_3 k_4 \theta_{SO_{3\,(ad)}^{2-}} \exp(\beta f E)\,(k_4 c_{OH^-}^2 + 2k_{-3})}}{k_3 k_4 c_{OH^-}} \quad (S40)$$

Finally, if Eqs. (S38) and (S40) are substituted into Eq. (S36), the overall sulfate production rate expression is obtained:

$$R_{SO_{4\,(ad)}^{2-}} = k_2 \theta_{SO_{3\,(ad)}^{2-}} \exp(\beta f E) \quad (S41)$$

Note that sulfate production depends on the rate constant of Step 2, sulfite, β and E. Consequently, this expression correlates to experimental data. Each pathway in Fig. S6 was analyzed through this approach establishing different steps as the rds, but only the mechanism in the main document can be related to our kinetic data.

Consequently, the overall sulfite electrooxidation rate expression is shown in Eq. (S42):

$$j = \frac{nF k_s^0 \theta_{SO_{3\,(ad)}^{2-}} \exp\left[-\frac{\beta n F (E - E^0)}{RT}\right]}{1 + \frac{k_s^0 \exp\left[-\frac{\beta n F (E - E^0)}{RT}\right]}{k_D}}; \quad k_D = J_D \exp\left[-\frac{Z_D}{RT}\right] \quad k_s^0 = k^0 \exp\left[-\frac{\beta n F E^0}{RT}\right] \quad (S42)$$

where fractional orders explain extent of adsorbed sulfite coverage which varies with potential.

4. Extended nomenclature

c_b Bulk concentration (mol m^{-3})

c_s Surface concentration (mol m^{-3})

D Diffusion coefficient (m^2 s^{-1})

E Electrode potential (V)

E^0 Standard electrode potential (V)

F Faraday's constant (96,487 A s^{-1} mol^{-1})

J_D Diffusional mass transfer pre-exponential factor

j Current density (A m^{-2})

j_k Kinetics-controlled current density (A m^{-2})

j_L Limiting current density (A m^{-2})

j_0 Exchange current density (A m^{-2})

K Equilibrium constant

k_D Diffusional mass transfer rate constant (m s^{-1})

k_s General heterogeneous rate constant (m s^{-1})

k_s^0 Heterogeneous rate constant (m s^{-1})

n Number of electrons transferred

n_i Reaction order of species *i*

R Gas constant (8.314 J mol^{-1} K^{-1})

T Absolute temperature (K)

Z_D Diffusional mass transfer activation energy (J mol^{-1})

Greek characters

α Cathodic charge transfer coefficient

β Anodic charge transfer coefficient

δ Diffusion layer thickness (m)

η Overpotential (V)

ν Kinematic viscosity of the solution (m^2 s^{-1})

θ_i Surface coverage of species *i*

ω Angular rotation rate (s^{-1})

Ω Formal activation energy (J mol^{-1})

References

[1] V.S. Protsenko, F.I. Danilov, J. Electroanal. Chem., 651 (2011) 105-110.
[2] J.-L. Burgot, Ionic Equilibria in Analytical Chemistry, Springer 2012.
[3] M. Bouroushian, Electrochemistry of Metal Chalcogenides, Springer-Verlag Berlin Heidelberg Berlin, 2010.
[4] J.A. O'Brien, J.T. Hinkley, S.W. Donne, S.E. Lindquist, Electrochim. Acta, 55 (2010) 573-591.
[5] T. Hunger, F. Lapicque, Electrochim. Acta, 36 (1991) 1073-1082.
[6] J.G. Bell, M. Dao, J. Wang, J. Electroanal. Chem., 816 (2018) 1-6.
[7] A.G. Zelinsky, B.Y. Pirogov, Electrochim. Acta, 231 (2017) 371-378.
[8] J. Lu, D.B. Dreisinger, W.C. Cooper, J. Appl. Electrochem., 29 (1999) 1161-1170.
[9] E. Skavås, T. Hemmingsen, Electrochim. Acta, 52 (2007) 3510-3517.
[10] K. Varga, P. Baradlai, A. Vértes, Electrochim. Acta, 42 (1997) 1143-1155.
[11] E. Skavas, M. Adriaens, T. Hemmingsen, Int. J. Electrochem. Sci., 1 (2006) 414-424.
[12] A.G. Zelinsky, Electrochim. Acta, 188 (2016) 727-733.
[13] J.A. Allen, G. Rowe, J.T. Hinkley, S.W. Donne, Int. J. Hydrogen Energy, 39 (2014) 11376-11389.
[14] C. Korzeniewski, W. McKenna, S. Pons, J. Electroanal. Chem. Interfacial. Electrochem., 235 (1987) 361-368.
[15] A.J. Appleby, B. Pichon, J. Electroanal. Chem. Interfacial. Electrochem., 95 (1979) 59-71.
[16] A.G. Zelinsky, Electrochim. Acta, 154 (2015) 315-320.
[17] S. Glasstone, A. Hickling, J. Chem. Soc., (1933) 829-836.
[18] W.M. Haynes, CRC Handbook of Chemistry and Physics, CRC Press/Taylor and Francis Group, Boca Raton, 2017.
[19] G. Lente, I. Fábián, Inorg. Chem., 43 (2004) 4019-4025.
[20] A. Bard, L. Faulkner, Electrochemical Methods: Fundamentals and Applications, Second ed., Wiley New York, 2000.
[21] J.O'M. Bockris, A.K.N. Reddy, Modern Electrochemistry, Plenum Press, New York, 1970.
[22] K. Scott, F. Goodridge, Electrochemical Process Engineering A Guide to the Design of Electrolytic Plant, Springer Science+ Business Media, New York, 1995.